Published in final edited form as:
Nano Lett. 2012 April 11; 12(4): 1757–1764. doi:10.1021/nl204596h.

Probing Dynamically Tunable Localized Surface Plasmon Resonances of Film-Coupled Nanoparticles by Evanescent Wave Excitation

Jack J. Mock[1,2], **Ryan T. Hill**[3], **Yu-Ju Tsai**[1,2], **Ashutosh Chilkoti**[3,4], and **David R. Smith**[1,2,*]

[1]Department of Electrical and Computer Engineering, Duke University, Durham, NC

[2]Center for Metamaterials and Integrated Plasmonics, Duke University, Durham, NC

[3]Center for Biologically Inspired Materials and Material Systems, Duke University, Durham, NC

[4]Department of Biomedical Engineering, Duke University, Durham, NC

Abstract

The localized surface plasmon resonance (LSPR) spectrum associated with a gold nanoparticle (NP) coupled to a gold film exhibits extreme sensitivity to the nano-gap region where the fields are tightly localized. The LSPR of an ensemble of film-coupled NPs can be observed using an illumination scheme similar to that used to excite the surface plasmon resonance (SPR) of a thin metallic film; however, in the present system, the light is used to probe the highly sensitive distance-dependent LSPR of the gaps between NPs and film rather than the delocalized SPR of the film. We show that the SPR and LSPR spectral contributions can be readily distinguished, and we compare the sensitivities of both modes to displacements in the average gap between a collection of NPs and the gold film. The distance by which the NPs are suspended in solution above the gold film is fixed via a thin molecular spacer layer, and can be further modulated by subjecting the NPs to a quasistatic electric field. The observed LSPR spectral shifts triggered by the applied voltage can be correlated with Angstrom scale displacements of the NPs, suggesting the potential for chip-scale or flow-cell plasmonic nanoruler devices with extreme sensitivity.

Keywords

Nanoparticles; gold film; localized surface plasmon resonance; doughnut; coupling; nanoruler; sensor

The use of surface plasmons associated with metal films and nanostructures for sensing has been well established over the past decades, resulting in well-known sensing configurations and devices. A particularly common sensing modality makes use of a thin metallic film deposited on the surface of a prism; light striking the film surface from the prism side, at an incident angle greater than the critical angle, undergoes total internal reflection (TIR) and can excite film surface plasmons via coupling to the evanescent fields associate with TIR light (1, 2). At wavelengths where this coupling is strong, light lost to the surface plasmons is manifested as a dip or resonance in the broadband reflection spectrum. Because the conditions for evanescent wave coupling to the surface plasmons of the film are so sensitive

*To whom correspondence should be addressed. drsmith@ee.duke.edu.

SUPPORTING INFORMATION AVAILABLE. Description of experimental methods, further discussion of key points in the manuscript, and Supporting Figures I and II are provided in the Supporting Information section. This material is available free of charge via the Internet at http://pubs.acs.org.

to the dielectric environment near the film, small changes in the local refractive index can lead to measurable changes and shifts in the resonance-like reflection spectrum.

The use of the surface plasmon resonance (SPR) associated with a thin metallic film as a means of detecting local refractive index changes from bio-molecular binding events is a technique that has now been commercialized to serve a sizable market for low cost, robust biological sensors, effective for small sample volumes (3). In sensor applications, the medium above the metal film is typically a buffer containing target analytes, which are captured at the functionalized metal surface. Small changes to the refractive index over the entire measured surface of the metal film, as a result of molecular binding events, affect both the preferred excitation angle and the resonance wavelength of the SPR. The effective refractive index changes of the detection volume due to molecular attachment are quite small, so maximizing the response of the SPR in either wavelength or excitation angle is desirable. Further enhancements to the sensitivity of SPR detection can be achieved by a variety of techniques, including binding plasmonic nanoparticles (NPs) to the analyte to enhance the change in refractive index as binding occurs (4–10); patterning the traditionally flat metal films (11–14); or modifying the metal surface with colloids (15, 16) to increase the refractive index sensitivity.

While SPR has been the predominant plasmonic sensing technique, a second emerging sensing modality is that of the localized surface plasmon resonance (LSPR) of a single metallic NP or an array of metallic nanostructures (17–24). As with SPR, analyte binding to the NP surface increases the local refractive index, shifting the plasmon resonance. In contrast to the SPR of films, the LSPR of a NP has the distinction that the local fields are much more tightly confined, effectively reducing the surface area that needs to be exposed to the reaction medium and the number of molecules required to achieve a measurable resonance shift. For example, in the case of a sharp tip or a gap between two NPs, strongly enhanced fields (orders of magnitude larger than the illumination field) occur that can be confined to a few cubic nanometers or less (25–27). Molecules that enter these high-field regions can produce relatively large spectral shifts in the LSPR. A disadvantage of the LSPR sensing technique is that the active volume corresponding to the local field enhancement regions of NPs is typically miniscule relative to the overall assay volume, so that the probability of detection by this method can be low, especially for low concentration assays.

Because the plasmonic interaction between closely spaced metallic NPs is so strong, an alternative LSPR sensing approach makes use of the spectral changes that occur on aggregation of two or more colloidal metal NPs. Selective, colorimetric detection was demonstrated early on in sandwich immunoassays of antibody coated gold colloids and later in hybridization experiments in which the presence of specific polynucleotide sequences were identified by a change in color of a colloid solution (28, 29). Even minute changes in the spacing between two interacting NPs can result in relatively large changes to the LSPR spectrum (27), such that a coupled NP pair can be used as an extremely sensitive *nanoruler* (30–35) capable of probing nanoscale molecular dynamics. The nanoruler concept also extends to the metal film-coupled NP (film-NP) system (36–41) studied here, where the associated LSPR shift exhibits a nonlinear dependence on the nanoscale gap between the NP and film. However, the metallic film independently supports delocalized surface plasmons that can also couple to the probing incident light and interfere with the specific detection of the LSPR from the film-NPs. In particular, light introduced in total internal reflection (TIR) can be used to interrogate the LSPR associated with a large population of the film-NPs, but will also invariably excite the SPR of the film. Further complicating matters is that the LSPR of the film-NPs and the SPR of the film do interact electromagnetically.

In the present work, we seek to combine the robustness and reliability of metal film-based SPR detection with the extreme sensitivity of the LSPR nanoruler. Though the illumination and detection scheme that we propose are cosmetically identical to that used in SPR systems, the spectrum we are interested in is that of the LSPR of the film-NPs—probed by the exponentially decaying, evanescent field that exists at the surface of the film from the TIR illumination. As a first step towards the development of a sensing platform, we investigate the gold NPs/molecular spacer layer/gold film system and correlate spectral shifts of the LSPR with changes in the film-NPs average gaps distance. We leverage information provided by Darkfield (DF) microscopy studies of the single film-NP to distinguish between SPR and LSPR resonances present in the TIR measurement of this system.

The optical properties of individual metal NPs have been extensively investigated using Darkfield (DF) microscopy (42–46). In prior work (47), individual metal film-coupled NPs were selected and their specific LSPR scattering spectra measured. With a microscope configured for DF epi-illumination, the incident light cannot directly excite the SPR of the metallic film and thus the LSPR of a film-NP can be investigated without interference from the SPR. However, while it might be desirable in certain circumstances to base LSPR detection on DF microscopy of a single nanostructure—for example when working at the single molecule level—it is also possible to resolve an averaged LSPR spectrum from ensembles of large numbers of NPs when the NPs are densely distributed (though noninteracting) and produce a uniform spectral response to their surroundings (48–51). There are several benefits of an ensemble measurement; one of which is that the interparticle spectral variations of single film-NPs are averaged out. Relying on the spectral response of a few single film-coupled NPs to predict the universal gap-distance dependence response can be misleading. Another benefit of an ensemble measurement is that simple and inexpensive chip-scale optical components can be used in place of an expensive and cumbersome microscope equipped with the high quality optics and detectors necessary to characterize single NPs.

We begin with dry (superstrate = air) DF microscope observations of the LSPR scattering from 60nm gold NPs (BBI International) electrostatically immobilized on a 30nm gold film (deposited on a Nexterion Glass B slide using a 5 nm chromium adhesion layer), using a single molecular spacer layer of poly(allylamine) hydrochloride (PAH, ~6 Angstrom average thickness, Fig 1 top left panel). As has been previously reported (47, 52–55), proximity to the gold film causes a substantial red-shift in the LSPR of the NP, which can be approximately explained by assuming the NP acts as a polarizable dipole interacting with its image dipole formed on the metal film. DF microscope images of the LSPR scattering from the film-NPs at various concentrations are shown in Figure 1, with an image of NPs deposited on a glass slide (n=1.5) for comparison. The images clearly demonstrate the effects of the gold film-NP coupling. In addition to a red-shifting of the NP LSPR, this coupling causes the dipole moment of the NP to become predominantly polarized normal to the surface of the film due to damping of the horizontal dipolar response, resulting in the doughnut-shaped diffraction limited point-spread-functions (PSFs) at the image plane. The plot in the right panel of Figure 1 shows representative scattering spectra, ranging from a single NP spectrum to spectra for optically irresolvable groupings of NPs, collected through a pinhole aperture from each of the samples depicted by the DF microscope images. The film-NPs samples were prepared using 0.05x, 0.1x, 0.2x and 1x colloid concentrations (56). A green LSPR, characteristic of a NP on a glass substrate, is red-shifted by more than 100nm when the NP is deposited on the gold film with a 6 Angstrom PAH spacer layer. Two striking features can be noted here. First, each film-NP displays reasonably uniform LSPR spectra and polarization response (red LSPR, doughnut-shaped scattering profile) across the gold film. This suggests that the 6 Angstrom average film-NP gap spacing is well

controlled over a large area, that the colloid size is reasonably mono-disperse, and that the metal film is sufficiently flat. Second, the film-NP LSPR is relatively insensitive (i.e. it does not shift significantly) to the NP surface coverage investigated here. Thus, ensemble measurements containing large numbers of densely packed film-NPs should provide access to the same, though slightly broadened, LSPR spectra as those collected from the single gold film-coupled NP.

An obvious method for characterization of the ensemble film-NPs—without using a microscope— is to measure the off-normal broadband reflectivity from the 'dry' (superstrate = air) surface. Due to the vertical orientation of the film-NP LSPR dipole (normal to the gold film) it is not useful to measure transmission or reflection with a light beam incident normal to the sample surface, for which the polarization of the incident electric field would be parallel to the plane of the film. Maximizing the component of light polarized parallel to the vertical dipole axis (normal to the plane of the film) will more efficiently excite the film-NP LSPR. Therefore, we measure the P-polarized reflectivity (electric field in the plane of incidence) of a collimated white light beam (Figure 2B inset: ~4mm diameter at the sample surface, 0.2 degree divergence, incidence angle = 70°), which reveals the extinction resulting from light either being scattered or absorbed by the film-NPs. In Figure 2A we plot this reflectivity for a series of samples prepared with a 1x NP concentration deposited on 30nm gold films that were pre-treated with layer-by-layer (LBL) assembled poly-electrolyte (PE) layers of various thicknesses as measured using an ellipsometer (56). The resulting curves demonstrate that the uniformity of the film-NP LSPR across all of the NPs in the measurement spot is sufficient to result in a single, though somewhat broadened, and distinctly distance-dependent resonance that non-linearly red-shifts (Figure 2B) with decreasing film-NPs average gap distance (d). Guided by a recent article by Baumberg et al (57), we have fit this data with a power law function ($y = 644.43 * d^{-0.058}$, R=.99147). While the same data from Figure 2B plotted on a log-log scale (56) does have a linear appearance – a signature of the power law function– over the entire range of gap distances studied in this article, this is not sufficient to determine that the system will continue to obey the power law in the asymptotic limit, implying an infinite spectral shift as the film-NP gap distance approaches zero. However in the region near the asymptotic limit, where *d* is just a few nanometers or less (circled region), the curve is steepest and spectral shifts are many nanometers for every 1 Angstrom change in the gap distance. In addition, the percentage extinction at the resonance peak associated with the LSPR of the film-NPs increases nonlinearly as the NPs approach the gold film (Figure 2C), an effect associated with but not equivalent to the power law dependence of the field enhancement (57) and corresponding to the effective doubling of the vertical dipole moments of the NPs coupled to their images. Once again in the region where *d* is just a few nanometers or less (circled), the amplitude of the measured LSPR signal is up to 7 times greater than the nearly uncoupled NPs—those sitting farther than 20nm from the film surface. The power law dependence of the spectral shift and the the local field enhancement are both important factors that reflect the strong near-field coupling between the NP and the film, as has been reported previously (36–41, 57). These characteristics suggest that an optimal thickness for the reactive spacer layer to be used in a film-NPs LSPR sensing platform should be on the order of a few nanometers or less to maximize response as the gap distance narrows.

By counting the number of NPs within a given field of view of an SEM image of the sample, we can determine the density for our standardized film-NPs sample preparations (Figure 3, right side). The highest concentration sample reported here (1x) has a 2.2% surface coverage relative to maximum packing density (touching spheres) and the average inter-particle center-to-center spacing for this sample is 400nm. In figure 3A we plot the off-normal P-polarized reflectivity of the samples for these NP concentrations. These spectra are normalized by the reflectivity of the bare gold film in order to remove the strong gold film

absorption effect at the blue end of the visible spectrum, and emphasize the LSPR. Note however, though it is possible for some of the energy of the film-NP LSPR to radiate into the 2d continuum of modes supported by the gold film, there is no direct coupling of the incident light to surface plasmons of the gold film. The LSPR of the film-NPs—excited by this illumination and accounting for the observed NP concentration-dependent resonance—is depicted in the lower right inset drawing of Figure 3A as dipolar red field lines surrounding the gold NPs. Based on the DF microscope measurements presented in Figure 1 and the ensemble reflectivity curves in Figure 3A, we can conclude that the NPs at this density are spaced at more than a sufficient distance to ensure that the vertically oriented (parallel side-by-side) dipoles induced in the film-coupled NPs do not strongly interact, since no blue-shift is observed (58). In fact, considering that the horizontal dipoles of the film-NPs are damped to the point of near cancellation, it would likely be possible to increase the NP density a bit further without significantly affecting the quality and position of the measured LSPR. However, the surface with the highest concentration NP preparation (1x) reported here, with the NPs spaced from the gold film by a single PAH layer of 6 Angstrom average thickness, provides an extinction of almost 30% of the incident light at the peak of the film-NP LSPR, which is adequate for our current application.

We have shown that the cumulative LSPR of a uniform population of 60 nm gold NPs coupled to a 30nm gold film can be characterized from a broad spectrum, off-normal P-polarized reflectivity measurement. However it is not convenient to measure the sample in this manner when it is covered with a flow cell and immersed in a fluid, as might be desirable for real-time biosensing in aqueous environments. A more optimal configuration is to collect the reflectivity spectrum using the evanescent field generated by total internal reflection (TIR) illumination at the substrate-fluid interface to couple to the NPs. We demonstrate this mode of detection by placing a flow cell (Grace Bio-Labs CoverWell™ Perfusion Chambers) on the film-NP sample (spacer layer: 1 PAH or ~6 Angstroms, concentration: 1x) and filling it with water, immersing the film-NPs. The slide is then placed atop a hemi-cylindrical fused silica lens (Britek Laser Optics) operating as an all-angle prism, with index matching oil between the slide and the lens. We direct a collimated 3mm diameter beam with a 3.4° divergence to the sample surface using a 70° angle of incidence (Figure 3B, inset top right), which meets the criteria for achieving TIR at the gold film/water interface. The resulting TIR reflectivity spectra (Figure 3B) are quite different from the reflectivity spectra taken from above the gold film (shown in Figure 3A). The TIR spectra of the film-NPs samples contain the delocalized gold film surface plasmon resonance (SPR), as confirmed by a spectrum of the gold film only (no NPs, light gray curve); for increasing concentrations of NPs, a second peak emerges corresponding to the LSPR of the film-NPs. The concentration of NPs deposited on the film determines both the amplitude of the LSPR dip and the magnitude of red-shift of the film's SPR.

The use of the evanescent field generated by TIR illumination to excite the film-coupled NPs is a key feature of the present configuration and ideal for real time sensing applications. However, care must be taken to distinguish the excitation of the delocalized SPR from the LSPR of the film-NPs, since the former is less sensitive and can interfere with the measurements. For clarity, the two contributions to the reflectivity spectrum are depicted in the lower left inset of Figure 3B, where both the gold film's SPR mode (brown field lines) and the film-NP's LSPR mode (red field lines) are illustrated. Reflected in TIR, the incident light has a wave vector large enough to directly couple to select gold film SPR modes and is the typical means of exciting surface plasmons in films. The incident light can also excite the LSPR of the film-NPs, since the evanescent decay length of the field is significantly larger than the combination of the film thickness (30nm) and the distance of the NPs from the film surface (~6 Angstroms). Under evanescent field excitation, the LSPR of the NPs and the delocalized SPR of the gold film are influenced by each other. The LSPR of each

individual NP is red-shifted and polarized by the gold film, while the evanescent field—which excites the NPs—also couples to the SPR of the gold film; thus, the spectrum of the excitation field represents a convolution of the incident light and the SPR. Likewise, the SPR of the gold film is red-shifted by the higher surface coverage of the NPs. However, as shown in Figure 3B, it is possible to spectrally distinguish the localized film-NP response from the delocalized SPR of the film (59–62). A comparison of Figures 3A and 3B reveals that as the NP concentration increases, the LSPR signal amplitude increases alongside the SPR of the film in the TIR reflectivity spectrum. Although, predictably the LSPR of the film-NPs in water (superstrate= 1.33, Figure 3B) is red-shifted due to the higher refractive index (17–24) from the LSPR measured 'dry' (superstrate=1.0, Figure 3A). For the measurement in 3B, we benefit from the fact that the LSPR peak signal is ~7 times greater for NPs that are spaced less than 1nm from, and thus strongly coupled to, the gold film. This intense coupling results in an LSPR response amplitude from a 2.2% NP surface coverage that is comparable to the strength of the film SPR. The presence of the two extinction dips is a promising sign for LSPR characterization using TIR reflectivity, and it should now be feasible to monitor a dynamically changing film-NP average gap distance (from the corresponding LSPR shift) in real-time in a wet cell. Based on the power law gap distance-dependence of the film-NPs presented in Figure 2, we expect the LSPR wavelength to shift many nanometers for every Angstrom of change in the average gap distance.

One method for changing the film-NPs average gap distance is to drive the suspended NPs towards and away from the gold film with an applied electric field. The gold colloids that are used in this experiment are citrate stabilized, resulting in a net negative charge per colloid in solution and are thus subject to electrophoretic forces. An electric field can be introduced to the system in the manner reported recently by Zocchi and Wang (63), who studied the elastic constants of globular proteins using evanescent wave scattering characterization to measure the displacement of gold NPs tethered to a gold film by a spring-like protein and driven by an oscillating electric field. Their method resulted in measurable changes of the evanescent wave scattering signal, indicating that NP motion is predictable based on electrophoretic force calculations. The force on the colloid from an applied electric field was used to controllably stretch and contract the molecular springs by fractions of an Angstrom. There are likely many complicating factors introduced by the electric field to the local film-NP environment such as ionic double layer formation at the metal surface and some swelling of the charged PE layer, as well as charge transfer effects perhaps operating on a slower timescale (64). However we believe that the basic principle of NP motion in response to the applied field is evident. By application of a voltage across the cell, we drive the NPs (tethered by a single PAH molecular layer) towards and away from the gold film as we monitor the LSPR and SPR peaks present in the TIR reflectivity spectrum. Copper tape serves as a top electrode and is fixed to the inner top surface of the flow cell (0.45 mm height) before it is placed over the film-NPs sample (1x NP concentration) and filled with 1/3X SSC buffer (50mM NaCl, 5mM trisodium citrate, pH 7.0). We then apply an AC voltage (0.5 Hz) between the gold film and the copper tape at the top of the flow cell using a square wave function generator (Figure 4A). For demonstration purposes, TIR spectra (Figure 4B) are first acquired from the sample for +/− 1 Volts (or +/− 2.2 V/mm in the flow cell). The LSPR of the film-NPs is blue shifted by approximately 30 nm when a negative voltage is applied to the gold film (Figure 4B, Polarity 2) compared to a positively charged gold film (Figure 4B, Polarity 1). Polarity 1 forces the NPs closer to the gold film, effectively reducing the average gap distance and increasing the coupling between the NPs and the film, both red-shifting the LSPR and increasing the amplitude of the LSPR response. Interestingly, the spectral position of the delocalized gold film SPR remains relatively unaffected by the displacement of the NPs. We attribute this lack of spectral shift to the relatively negligible change in the refractive index caused by the sub-nanometer motion of the 60 nm diameter NPs within the extended region above the gold film occupied by the

surface plasmons. While a +/− 2.2 V/mm quasistatic applied field results in an impressive LSPR spectral shift, we found that the LSPR began to degrade after just a few minutes of cycling between polarities. Applying a constant voltage also rapidly and irreversibly degraded the LSPR response. We believe that this most likely represents NPs detaching from the film surface, but could also be a result of either microscopic physical deformation of the polymer layer due to delamination; bubble formation from electrolysis; or some combination of these mechanisms.

From these results it can be concluded that the spectral position of the LSPR is a significantly more sensitive metric for monitoring the film-NPs average gap dimension than the spectral position of the delocalized SPR. Conveniently, these TIR measurements of the LSPR can be done in real time via evanescent field sensing in a wet cell without having to use a microscope. In Figure 5 we plot the evolution of the LSPR peak position (taken from sequential spectra sampled approximately every 350 ms.) over a number of voltage cycles. For these series we applied only a +/− 500 mV (+/− 1.1 V/mm) square wave (Figure 5A) to reduce the amplitude and duration of the electrophoretic force on the NPs and to avoid sample destruction. This lower field results in a smaller spectral shift than in Figure 4B but preserves the integrity of the sample. In addition to the PAH layer used throughout this article, we introduce additional molecular spacer layers using self-assembled monolayers (SAMs) of 11-amino-1-undecanethiol (we refer to this as “amine thiol” or “C11 amine thiol”) as well as SAMs of an amine thiol molecule containing the same C11 segment plus an additional segment of 6 ethylene glycol units in between the terminal thiol and amine groups (we refer to this as “EG6 C11 amine thiol”, see 56 for details of SAM formation).

For the three samples presented in Figure 5, ellipsometric measurements suggest that the three layers have distinct ‘dry’ (superstrate = air) thicknesses (PAH – 5.08 Angstroms, C11 amine thiol – 10.13 Angstroms, C11 EG6 amine thiol 18.28 Angstroms). While the ellipsometer suggests precise values for the thicknesses, the implied sub-Angstrom accuracy cannot be relied on as a local measure of thickness, which assuredly has a variation well beyond the stated precision, as discussed below. As can be seen in Figure 5B, C and D where the LSPR spectral position (solid lines) of the film-coupled NPs on the three layer types are plotted – both the central LSPR position and the magnitude of spectral shift triggered by the +/− 500mV field depend on the layer type. The LSPR of the PAH layer (Figure 5E, the thinnest spacer layer) is centered near 709nm – the most red-shifted LSPR of the three layers – and shifts by +/− 3 nm from the applied field. In contrast, for the much thicker 11 EG6 amine thiol layer (Figure 5G), the LSPR is centered near 676nm and the LSPR only shifts by approximately +/− 0.5 nm from the applied field. This non-linear LSPR response is what we expect at these very small gap dimensions. The smaller the dimension of the gap between the NP and the film the more red-shifted the LSPR and the more sensitive the LSPR position becomes to NP motion.

It is useful to remember that the LSPR position measured here represents the cumulative response from millions of film-coupled NPs in the beam spot. We are averaging out the statistical variations of the gap dimensions from each of the individual NPs. However, using this averaged LSPR response we can make some rough estimates of the average NP motion induced by the applied field. We stress that these estimates are in no way meant to be precise predictions of the gap dimensions. We rely on initial estimates of the polymer layer thickness provided by the ellipsometer which is operating near the limit of its ability to resolve such sub-nanometer layers, and is making measurements of the dry layer rather than the hydrated layer. Nevertheless, estimating the NP displacement from the LSPR shift at these Angstrom scale dimensions can be accomplished using the distance dependence calibration from Figure 2B. Since the data in Figure 2B come from a dry sample, to apply it to this data set we must adjust the power law fit function to account for the LSPR red-shift

from fluid immersion. A complete description of this calculation can be found in the supporting information (56). Briefly, we determine the average gap dimension of each of the fim-NPs samples using ellipsometer layer thickness measurements (we add 40% swelling factor which is expected to occur for the PAH layer during immersion, 56), we measure the LSPR position from the immersed samples at 0V and then we plot these points for the three samples on the graph from Figure 2B and vertically offset (red-shift) the power law function to force it through the median position of these points. The result is an adjusted power law distance dependence equation ($y = 699.43 * d^{-0.058}$). Using this equation, the spectral position of the LSPR (dynamically shifted by the applied field), if constrained along the line representing the power law curve fit adjusted for the higher index superstrate, can be converted to gap dimension. This estimated gap dimension is plotted in Figure 5B, C and D (dashed lines, right axis) for the three layer types. Once again, we confirm that applying a positive potential at the gold film (Polarity 1) drives the NP towards the gold film, reducing the gap dimension and red-shifting the LSPR, while applying a negative potential to the gold film (Polarity 2) has the opposite effect. The charged nature and conformation of the PAH layer makes it distinct from the amine thiol layer types and possibly more susceptible to swelling from ionic uptake during applied voltage cycles. Additionally, the EG6 amine thiol layer may respond in a different manner than the C11 amine thiol given the EG6 amine thiol molecule is composed of both a hydrophobic and a hydrophilic domain whereas the amine thiol is, aside from the terminal functional groups, mostly hydrophobic. Ascertaining the extent of the differences in layer response at these scales would be quite difficult. However, we would expect that ionic uptake would tend to amplify the NP motion on the PAH layer compared to the NP motion on amine thiol molecular layers. Keeping in mind that our NP displacement calculations include a number of rough estimates, what we find from our data is that the applied field appears to drive the NP displacement to a varying degree with each layer type; with PAH, C11 amine thiol, and C11 EG6 amine thiol producing average NP displacements of 1.07, 0.66, and 0.47 Angstroms respectively. Thus, from these data the thinner and less ordered PAH layer appears to facilitate a NP displacement that is roughly 2 times greater than that found from a relatively more ordered and thicker C11 EG6 amine thiol layer.

Our motivation for using an applied electric field to move the NPs up and down near the metal film is to demonstrate that the LSPR measured using TIR is indeed distinct from the delocalized SPR of the film and can be controlled independently by changing the gap dimension of the film-NPs. While the two resonances can influence each other, their responses to changing physical conditions are distinct. With the correct NP density and when the spacer dimension between the NPs and the film is on the order of a few nanometers causing the amplitude and spectral response of the LSPR to be dramatically enhanced, the LSPR can be characterized using simple TIR measurements similar to those used in commercial SPR instruments. In contrast to more common SPR sensing modalities, evanescent sensing of the film-NPs LSPR will transition readily to a chip-based dielectric waveguide platform and provide a component of information not strictly dependent on the local refractive index. The LSPR is exquisitely sensitive to the average gap dimension of the film-NPs; this metric will present an opportunity for making real time nanoruler measurements of molecular dynamics from a potentially broad array of biomolecules and inorganics that can be integrated into the gap region.

Supplementary Material

Refer to Web version on PubMed Central for supplementary material.

Acknowledgments

This work was partially supported by NIH grant R21EB009862. DRS and JJM acknowledge partial support from the Air Force Office of Scientific Research (Contract No. FA9550-09-1-0562). RTH also acknowledges support by Award Number F32EB009299 from the NIH NIBIB. Dr. Yaroslav Urzhamov provided theoretical support. We would also like to thank Dr. Orlin D. Velev for providing insight on the surface chemistry of the system under an applied potential. Greg J. Nusz provided MATLAB code for finding centroids of plasmon resonance peaks. Content is solely the responsibility of the authors and does not represent the official views of the funding agencies.

REFERENCES AND NOTES

1. Raether, H. Surface Plasmons. Hohler, G., editor. Springer; Berlin: 1988.
2. Barnes WL, Dereux A, Ebbesen TW. Surface plasmon subwavelength optics. Nature. 2003; 424:824–830. [PubMed: 12917696]
3. Baird CL, Myszka DG. Current and emerging commercial optical biosensors. J Mol Recognit. 2001; 14:261–268. [PubMed: 11746946]
4. He L, Smith EA, Natan MJ, Keating CD. The distance-dependence of colloidal Au-amplified surface plasmon resonance. J Phys Chem. 2004; 108:10973–10980.
5. Lu G, Cheng B, Shen H, Zhou Y, Chen Z, Yang G, Tillement O, Roux S, Perriat P. Fabry-Perot type sensor with surface plasmon resonance. App Phys Lett. 2006; 89:223904.
6. Wang J, Munir A, Li Z, Zhou HS. Aptamer-Au NPs conjugates-enhanced SPR sensing for the ultrasensitive sandwich immunoassay. Biosensors and Bioelectronics. 2009; 25:124–129. [PubMed: 19592231]
7. Law WC, Yong KT, Baev A, Hu R, Prasad PN. Nanoparticle enhanced surface plasmon resonance biosensing: Application of gold nanorods. Optics Express. 2009; 17:19041–19046. [PubMed: 20372639]
8. Sim HR, Wark AW, Lee HJ. Attomolar detection of protein biomarkers using biofunctionalized gold nanorods with surface plasmon resonance. Analyst. 2010; 135:2528–2532. [PubMed: 20725693]
9. Mustafa DE, Yang T, Xuan Z, Chen S, Tu H, Zhang A. Surface plasmon coupling effect of gold nanoparticles with different shape and size on conventional surface plasmon resonance signal. Plasmonics. 2010; 5:221–231.
10. Law WC, Yong KT, Baev A, Prasad PN. Sensitivity improved surface plasmon resonance biosensor for cancer biomarker detection based on plasmonic enhancement. ACS Nano Online ASAP. 2011
11. Wark AW, Lee HJ, Qavi AJ, Corn RM. Nanoparticle-enhanced diffraction gratings for ultrasensitive surface plasmonbiosensing. Anal Chem. 2007; 79:6697–6701. [PubMed: 17676761]
12. Yang X, Liu D. Sensitivity enhancement of surface plasmon resonance sensors through planar metallic film closely coupled to nanogratings. Chinese Optics Lett. 2007; 5:563–565.
13. Mistark PA, Park S, Yalcin SE, Lee DH, Yavuzcetin O, Tuominen MT, Russell TP, Achermann M. Block-copolymer-based plasmonic nanostructures. A C S Nano. 2009; 3:3987–3992.
14. Vazquez-Mena O, Sannomiya T, Villanueva LG, Voros J, Brugger J. Metallic nanodot arrays by stencil lithography for plasmonic biosensing applications. A C S Nano Online ASAP. 2011
15. Rueda A, Stemmler M, Bauer R, Fogel Y, Mullen K, Kreiter M. Localized plasmons seen by propagating surface plasmons: unique determination of their dielectric response. J Phys Chem. 2008; 112:14801–14811.
16. Uchiho Y, Shimojo M, Furuya K, Kajikawa K. Optical response of gold nanoparticle-amplified surface plasmon resonance spectroscopy. J Phys Chem. 2010; 114:4816–4824.
17. Raschke G, Kowarik S, Franzl T, Sonnichsen C, Klar ALTA, Feldman J. Biomolecular recognition based on single gold nanoparticle light scattering. Nanoletters. 2003; 3:935–938.
18. McFarland AD, Van Duyne RP. Single silver nanoparticles as real-time optical sensors with zeptomole sensitivity. Nanoletters. 2003; 3:1057–1062.
19. Tam F, Moran C, Halas N. Geometrical parameters controlling sensitivity of nanoshell plasmon resonances to changes in dielectric environment. J Phys Chem. 2004; 108:17290–17294.

20. Raschke G, Brogl S, Susha AS, Rogach AL, Klar TA, Feldman J. Gold nanoshells improve single nanoparticle molecular sensors. Nanoletters. 2004; 4:1853–1857.
21. Yonzon CR, Jeoung E, Zou S, Schatz GC, Mrksich M, Van Duyne RP. A comparative analysis of localized and propagating surface plasmon resonance sensors: The binding of Concanavalin A to a monosaccharide functionalized self-assembled monolayer. J Am Chem Soc. 2004; 126:12669–12676. [PubMed: 15453801]
22. Miller MM, Lazarides AA. Sensitivity of metal nanoparticle surface plasmon resonance to the dielectric environment. J Phys Chem. 2005; 109:21556–21565.
23. Nusz GJ, Curry A, Marinakos SM, Wax A, Chilkoti A. Rational selection of gold nanorod geometry for label-free plasmonic biosensors. A C S Nano. 2009; 3:795–806.
24. Chen S, Svedendahl M, Van Duyne RP, Kall M. Plasmon-enhanced colorimetric ELISA with single molecule sensitivity. Nanoletters. 2011; 11:1826–1830.
25. Kottmann JP, Martin OJF, Smith DR, Schultz S. Plasmon resonances of silver nanowires with a nonregular cross section. Phys Rev B. 2001; 64:235402.
26. Hao E, Schatz GC. Electromagnetic fields around silver nanoparticles and dimers. J Chem Phys. 2004; 120:357–366. [PubMed: 15267296]
27. Romero I, Aizpurua J, Bryant GW, Garcia de Abajo FJ. Plasmons in nearly touching metallic nanoparticles: singular response in the limit of touching dimers. Optics Express. 2006; 14:9988–9999. [PubMed: 19529393]
28. Leuvering JHW, Thal PJHM, Van Der Waart M, Schuurs AHWM. Sol Particle Immunoassay (SPIA). J Immunoassay. 1980; 1:77–91. [PubMed: 7014638]
29. Elghanian R, Storhoff JJ, Mucic RC, Letsinger RL, Mirkin CA. Selective colorimetric detection of polynucleotides based on the distance-dependent optical properties of gold nanoparticles. Science. 1997; 277:1078–1081. [PubMed: 9262471]
30. Tokareva I, Minko S, Fendler JH, Hutter E. Nanosensors based on responsive polymer brushes and gold nanoparticle enhanced transmission surface plasmon resonance spectroscopy. J Am Chem Soc. 2004; 126:15950–15951. [PubMed: 15584714]
31. Sonnichsen C, Reinhard BM, Liphardt J, Alivisatos AP. A molecular ruler based on plasmon coupling of single gold and silver nanoparticles. Nature Biotechnology. 2005; 23:741–745.
32. Liu GL, Yin Y, Kunchakarra S, Mukherjee B, Gerion D, Jett SD, Bear DG, Gray JW, Alivisatos AP, Lee LP, Chen FF. A nanoplasmonic molecular ruler for measuring nuclease activity and DNA footprinting. Nature Nanotech. 2006; 1:47–52.
33. Lee J, Hernandez P, Lee J, Govorov AO, Kotov N. Exciton-plasmon interactions in molecular spring assemblies of nanowires and wavelength-based protein detection. Nature Materials. 2007; 6:291–295.
34. Gupta S, Uhlmann P, Agrawal M, Chapuis S, Oertel U, Stamm M. Immobilization of silver nanoparticles on responsive polymer brushes. Macromolecules. 2008; 41:2874–2879.
35. Yockell-Lelievre H, Gingras D, Vallee R, Ritcey AM. Coupling of localized surface plasmon resonance in self-organized polystyrene-capped gold nanoparticle films. J Phys Chem. 2009; 113:21293–21302.
36. Nordlander P, Le F. Plasmonic structure and electromagnetic field enhancements in the metallic nanoparticle-film system. App Phys B. 2006; 84:35–41.
37. Ikeda K, Sato J, Fujimoto N, Hayazawa N, Kawata S, Uosaki K. Plasmonic enhancement of raman scattering on non-serrs-active platinum substrates. J Phys Chem. 2009; 113:11816–11821.
38. Hill RT, Mock JJ, Urzhumov Y, Sebba DS, Oldenburg SJ, Chen S-Y, Lazarides AA, Chilkoti A, Smith DR. Leveraging nanoscale plasmonic modes to achieve reproducible enhancement of light. Nanoletters. 2010; 10:4150–4154.
39. Kim NH, Lee SJ, Moskovits M. Aptamer-mediated surface-enhanced raman spectroscopy intensity amplification. Nanoletters. 2010; 10:4181–4185.
40. Gehan H, Fillaud L, Chehimi MM, Aubard J, Hohenau A, Felidj N, Mangeney C. Thermo-induced electromagnetic coupling in gold/polymer hybrid plasmonic structures probed by surface-enhanced raman scattering. A C S Nano. 2010; 4:6491–6500.
41. Ikeda K, Suzuki S, Uosaki K. Crystal face dependent chemical effects in surface-enhanced raman scattering at atomically defined gold facets. Nanoletters. 2011; 11:1716–1722.

42. Yguerabide J, Yguerabide EE. Light-scattering submicroscopic particles as highly fluorescent analogs and their use as tracer labels in clinical and biological applications. Anal Biochem. 1998; 262:157–176. [PubMed: 9750129]
43. Schultz S, Smith DR, Mock JJ, Schultz DA. Single-target molecule detection with nonbleaching multicolor optical immunolabels. Proc Nat Acad Sci. 2000; 97:996–1001. [PubMed: 10655473]
44. Sonnichsen C, Geier S, Hecker NE, von Plessen G, Feldmann J, Diltbacher H, Lamprecht B, Krenn JR, Aussenegg FR, Chan VZ-H, Spatz JP, Moller M. Spectroscopy of single metallic nanoparticles using total internal reflection microscopy. App Phys Lett. 2000; 77:2949–2951.
45. Sonnichsen C, Franzl T, Wilk T, von Plessen G, Feldman J. Drastic reduction of plasmon damping in gold nanorods. Phys Rev Lett. 2002; 88:077402. [PubMed: 11863939]
46. Sonnichsen C, Alivisatos AP. Gold nanorods as novel nonbleachingplasmon-based orientation sensors for polarized single-particle microscopy. Nanoletters. 2005; 5:301–304.
47. Mock JJ, Hill RT, Degiron A, Zauscher S, Chilkoti A, Smith DR. Distance-dependent plasmon resonant coupling between a gold nanoparticle and gold film. Nano Lett. 2008; 8:2245–2252. [PubMed: 18590340]
48. Nath N, Chilkoti A. A colorimetric gold nanoparticle sensor to interrogate biomolecular interactions in real time on a surface. Anal Chem. 2002; 74:504–509. [PubMed: 11838667]
49. Rindzevicius T, Alaverdyan Y, Dahlin A, Hook F, Sutherland DS, Kall M. Plasmonic sensing characteristics of single nanometric holes. Nanoletters. 2005; 5:2335–2339.
50. Willets KA, Van Duyne RP. Localized surface plasmon resonance spectroscopy and sensing. Annu Rev Phys Chem. 2007; 58:267–297. [PubMed: 17067281]
51. Huang C, Bonroy K, Reekmans G, Laureyn W, Verhaegen K, De Vlaminck I, Lagae L, Borghs G. Localized surface plasmon resonance biosensor integrated with microfluidic chip. Biomed Microdevices. 2009; 11:8893–901.
52. Leveque G, Martin OJF. Tunable composite nanoparticle for plasmonics. Optics Lett. 2006; 31:2750–2752.
53. Papanikolaou N. Optical properties of metallic nanoparticle arrays on a thin metallic film. Phys Rev B. 2007; 75:225426.
54. Rueda A, Stemmler M, Bauer R, Mullen K, Fogel Y, Kreiter M. Optical resonances of gold nanoparticles on a gold surface: quantitative correlation of geometry and resonance wavelength. New Journal of Physics. 2008; 10:113001.
55. Hu M, Ghoshal A, Marquez M, Kik PG. Single particle spectroscopy study of metal-film-induced tuning of silver nanoparticle plasmon resonances. J Phys Chem. 2010; 114:7509–7514.
56. Supporting Online Materials
57. Huang FM, Wilding D, Speed JD, Russell AE, Bartlett PN, Baumberg JJ. Dressing plasmons in particle-in-cavity architectures. NanoLetters. 2011; 11:1221–1226.
58. Su K-H, Wei Q-H, Zhang X, Mock JJ, Smith DR, Schultz S. Interparticle coupling effects on plasmon resonances of nanogold particles. NanoLetters. 2003; 3:1087–1090.
59. Leveque G, Martin OJF. Optical interactions in a plasmonic particle coupled to a metallic film. Optics Express. 2006; 14:9971–9981. [PubMed: 19529391]
60. Kelf TA, Sugawara Y, Cole RM, Baumberg JJ. Localized and delocalized plasmons in metallic nanovoids. Phys Rev B. 2006; 74:245415.
61. Le F, Lwin NZ, Halas NJ, Nordlander P. Plasmonic interactions between a metallic nanoshell and a thin metallic film. Phys Rev B. 2007; 76:165410.
62. Brunazzo D, Descrovi E, Martin OJF. Narrowband optical interactions in a plasmonic nanoparticle chain coupled to a metallic film. Optics Letters. 2009; 34:1405–1407. [PubMed: 19412287]
63. Wang Y, Zocchi G. Elasticity of globular proteins measured from the ac susceptibility. Phys Rev Lett. 2010; 105:238104. [PubMed: 21231509]
64. Chapman R, Mulvaney P. Electro-optical shifts in silver nanoparticle films. Chem Phys Lett. 2001; 349:358–362.

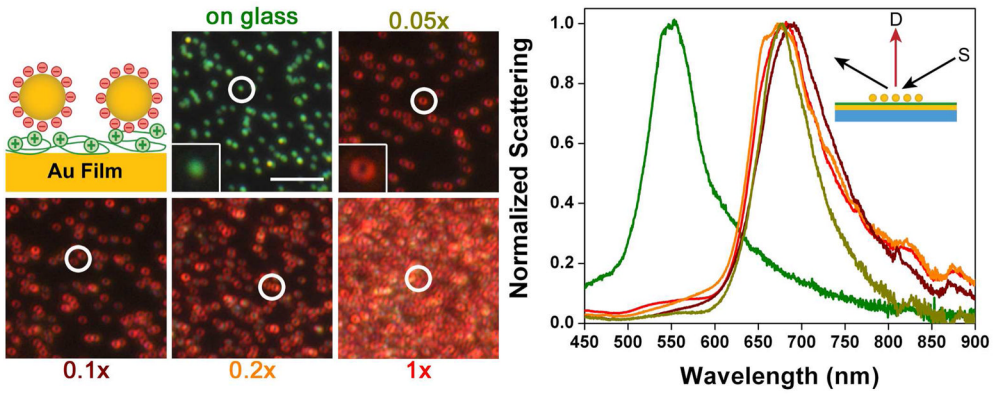

Figure 1.

Darkfield (DF) microscopy study of the uniformity of the localized surface plasmon resonance (LSPR) of 60nm gold NPs deposited on a 30nm gold film (5nm Cr adhesion layer), and the influence of NP density. NPs are attached to the gold film via electrostatic attraction to a single self assembled PAH molecular layer, resulting in an average gap distance of 6 Angstroms (top left panel drawing). This drawing is not to scale, as the actual gap dimension is less than 1/60 of the NP diameter. DF microscope color images of the gold NPs at reproducible standardized deposition concentrations are shown: on glass (5 μm scale bar), 0.05x on gold film, 0.1x on gold film, 0.2x on gold film, 1x on gold film. Insets highlight the doughnut image resulting from the gold film polarization effect on the NP scattering. The white circle represents approximately the aperture size through which the scattering spectra are collected. B) Representative scattering spectra acquired from film-NPs samples at concentrations of 0.05x (olive), 0.1x (maroon), 0.2x (orange), 1x (red) and for the same gold NPs on a glass slide (green) for comparison. Plot inset: Ray diagram describing the un-polarized illumination and collection conditions for DF microscope LSPR scattering characterization (S: source, D: detector).

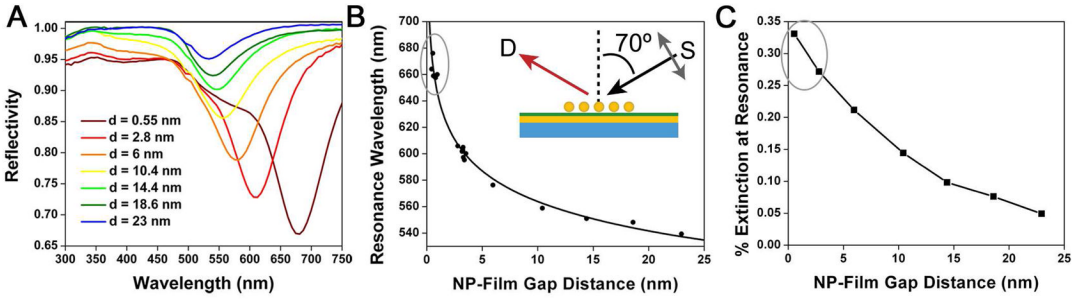

Figure 2.

Reflectivity measurements (Fig B inset: experimental geometry) of the surface of the 30nm gold film prepared with a 1x concentration 60nm gold NP surface coverage reveal the cumulative LSPR of a large number of NPs in the beam spot. A) Reflectivity curves for film-NPs samples (all at the same 1x NP concentration) with LBL assembled poly-electrolyte (PE) multi-layers used to space NPs at varying gap distances (d). There are two distinct distance-dependent trends apparent, which are shown in B and C. B) The LSPR position (calculated by centroid- center of mass of the bottom 80% of the resonance peaks shown in A) red-shifts, following a power law, with decreasing film-NPs average gap distance. A curve fit with the function $y = 644.43 * d^{-0.058}$, (R=.99147, where y= LSPR wavelength), is shown with the data. C) The peak amplitude of the LSPR response also increases with decreasing film-NPs average gap distance. The film-NPs based LSPR nanoruler sensor we propose would operate in the regime (gray ovals) where both the amplitude and the spectral response of the signal are strongest.

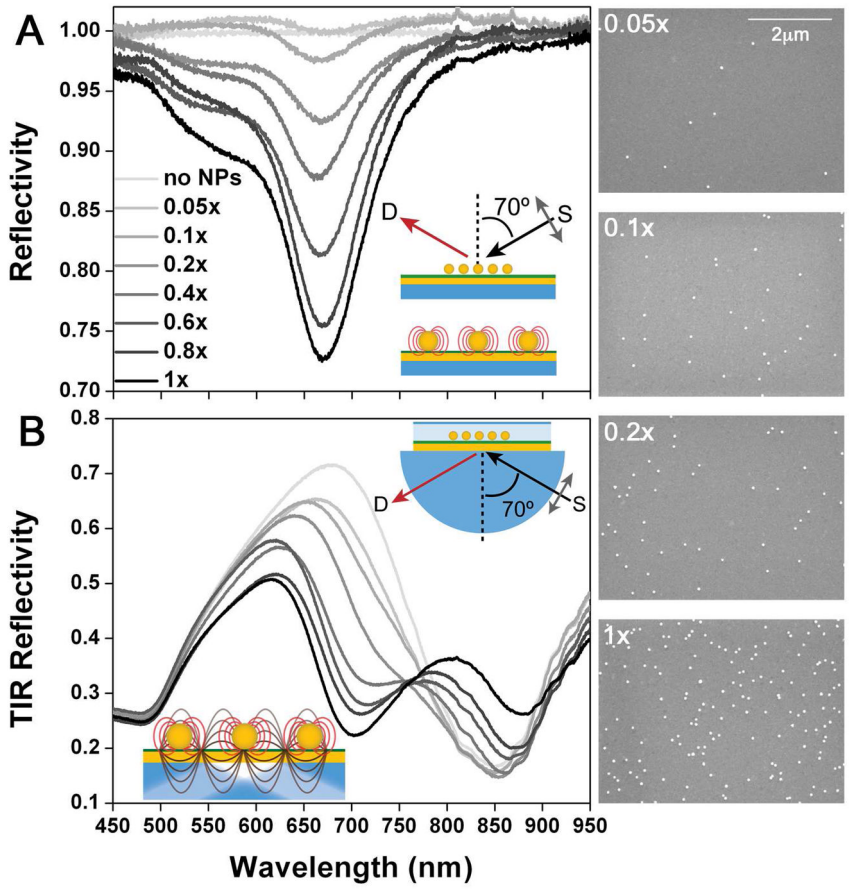

Figure 3.

Reflectivity measurements of the film-coupled NPs illustrate NP concentration dependence of the LSPR amplitude. All film-NPs samples shown here have a single PAH spacer layer that averages 6 Angstroms in thickness. A) Reflectivity spectra (normalized by bare gold film reflectivity) at various NP concentrations: using the same geometry (upper inset drawing top) as described in Figure 2. This illumination geometry results in excitation of the LSPR (red field lines) of the film-NPs, as drawn in the bottom of the upper inset, and cannot directly couple to the gold film SPR. B) TIR spectra from the same samples (normalized by glass slide reflectivity) using the collection geometry and 70° off-normal P-polarized sub-surface illumination described in the top right inset. In this case, we have fixed a flow cell to the top of each of the samples and filled it with water, altering the local refractive index from n=1.0 (air) to n=1.33. As represented in the lower left inset drawing: TIR geometry illumination results in evanescent component excitation of both the SPR (brown field lines) of the gold film and LSPR (red field lines) of the film-NPs. With no NPs present, there is a strong dip in the reflectivity at 850 nm associated with SPR excitation. However, as the NP concentration grows, one can observe both the appearance of an LSPR response and the red-shifting of the film SPR. Scanning electron microscope (SEM) images of the standardized film-NPs concentrations are shown at right. Particle counting reveals that the surface coverage (relative to maximum packing density) of the NPs are 1x = 2.2%, 0.2x = 0.42%, 0.1x = 0.22% and 0.05x = 0.11%.

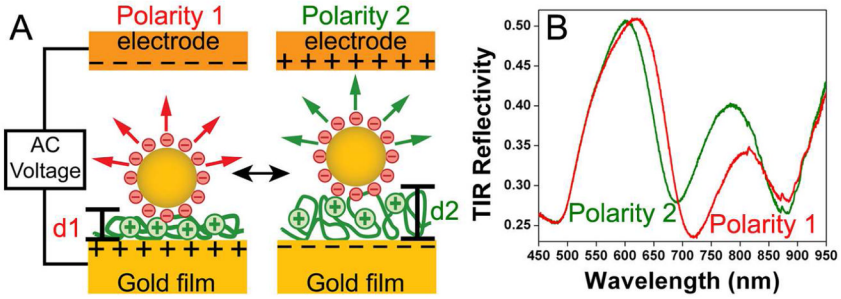

Figure 4.

The TIR spectrum of the film-NPs (prepared with 1x concentration NP surface coverage and a single PAH spacer layer on a 30nm gold film) displays an LSPR shift when the negatively charged citrate stabilized gold NPs are driven up and down by electrophoretic forces in an applied electric field. The experimental geometry of the signal collection is equivalent to Figure 3B. A) A +/− 1 Volt square wave (0.5Hz) is applied between the gold film and the top of the flow cell. We define Polarity 1 as a positive voltage at the gold film and Polarity 2 as a negative voltage at the gold film. B) Spectra acquired during Polarity 1 (1 Volt, 2.2V/mm) phase reflect a very large (~30nm) red-shift and amplitude increase of the LSPR compared to the Polarity 2 phase. This is understood to be the negatively charged NPs migrating away from the negative electrode and towards the positive gold film in Polarity 1, reducing the average film-NPs gap distance and increasing the plasmonic coupling. Conversely, for Polarity 2 the blue-shifting LSPR represents NP displacement away from the gold film. The spectral position of the SPR remains relatively unchanged.

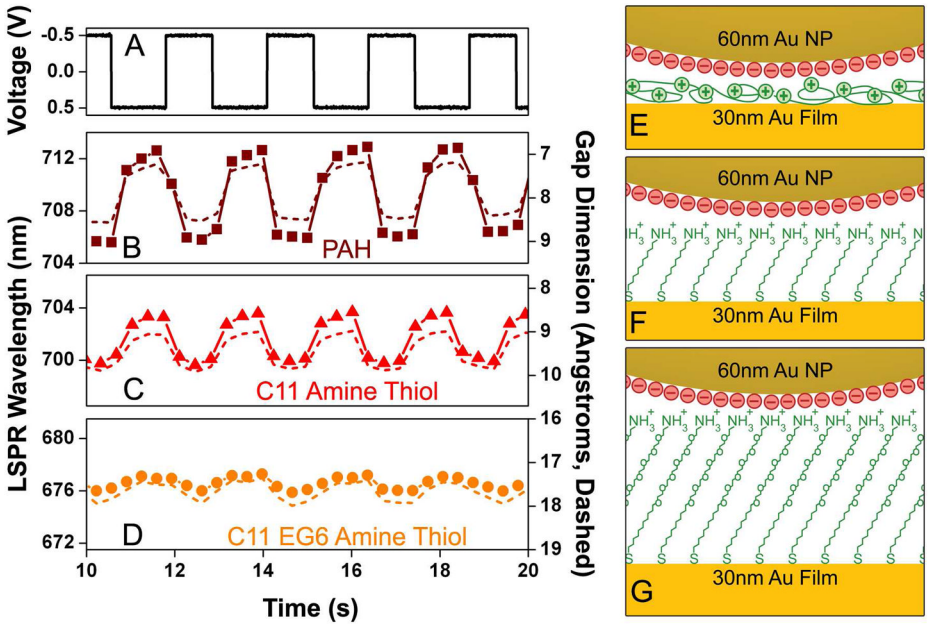

Figure 5.

The LSPR peak position of the film-NPs (prepared with 1x concentration NPs) oscillates at the frequency of the applied AC field as the gold NPs are driven up and down primarily by an electrophoretic force. The experimental geometry of the signal collection is equivalent to Figure 4. A) A +/− 500mV square wave (0.5Hz) is applied between the gold film and the top of the flow cell (here V represents the voltage at the gold film). The LSPR peak position (solid line, including data points) is plotted along with the estimated gap distance (dashed line) for film-coupled NPs attached via a single PAH layer (B, E), a self-assembled monolayer (SAM) of 11-amino-1-undecanethiol (C11 amine thiol, C, F) and a SAM of C11 EG6 amine thiol (D, G).